Structural insights into the mechanism of c-di-GMP–bound YcgR regulating flagellar motility in *Escherichia coli*

Received for publication, June 11, 2019, and in revised form, November 29, 2019 Published, Papers in Press, December 13, 2019, DOI 10.1074/jbc.RA119.009739

Yan-Jie Hou[‡], Wen-Si Yang[‡], Yuan Hong[‡], Ying Zhang[‡], Da-Cheng Wang[‡1], and De-Feng Li[§2]

From the [‡]National Laboratory of Biomacromolecules, CAS Center for Excellence in Biomacromolecules, Institute of Biophysics, and the [§]State Key Laboratory of Microbial Resources, Institute of Microbiology, Chinese Academy of Sciences, Beijing 100101, China

Edited by Chris Whitfield

The motile-sessile transition is critical for bacterial survival and growth. Cyclic-di-GMP (c-di-GMP) plays a central role in controlling this transition and regulating biofilm formation via various effectors. As an effector of c-di-GMP in *Escherichia coli* and related species, the PilZ domain–containing protein YcgR responds to elevated c-di-GMP concentrations and acts on the flagellar motor to suppress bacterial motility in a brakelike fashion, which promotes bacterial surface attachment. To date, several target proteins within the motor, MotA, FliG, and FliM, along with different regulatory mechanisms have been reported. However, how YcgR acts on these components remains unclear. Here, we report that activated YcgR stably binds to MotA at the MotA-FliG interface and thereby regulates bacterial swimming. Biochemical and structural analyses revealed that c-di-GMP rearranges the PilZ domain configuration, resulting in the formation of a MotA-binding patch consisting of an R*XXX*R motif and the C-tail helix α3. Moreover, we noted that a conserved region in the YcgR-N domain, which is independent of MotA interaction, is necessary for motility regulation. On the basis of these findings, we infer that the YcgR-N domain is required for activity on other motor proteins. We propose that activated YcgR appends to MotA via its PilZ domain and thereby interrupts the MotA-FliG interaction and simultaneously interacts with other motor proteins via its YcgR-N domain to inhibit flagellar motility. Our findings suggest that the mode of interaction between YcgR and motor proteins may be shared by other PilZ family proteins.

Cyclic-di-GMP (c-di-GMP)[3] is a ubiquitous bacterial second messenger that plays a central regulatory role in diverse biological processes (1, 2). The different levels of c-di-GMP concentration produce diverse output signals to regulate various kinds of processes (3). It has been shown to control the motile-sessile transition, in which bacterial motility is regulated by low c-di-GMP levels, along with surface attachment and biofilm formation, which are promoted by high levels (4). The concentration of c-di-GMP is controlled by GGDEF domain–containing diguanylate cyclases (DGCs) and EAL or HD-GYP domain-containing phosphodiesterases (PDEs) (5, 6). Numerous GGEDF/EAL/HD-GYP domain–containing proteins have been identified across different bacterial genomes (*e.g.* 29 in *Escherichia coli*) (7). Notably, only the PDE YhjH (and probably YliE) (8, 9) and four DGCs, YfiN, YegE, YedQ, and YddV, exclusively regulate the c-di-GMP concentration that controls bacterial motility in *E. coli* (7).

The various functions of c-di-GMP rely on its binding to respective effectors and then acting on their specific downstream targets (1). The effectors mainly include transcription factors, riboswitches, and degenerate GGDEF or EAL domain and PilZ domain proteins (2, 4), among which the PilZ domain proteins were the first discovered (10) and are the most well-studied. One PilZ domain protein in *E. coli* (8, 10), YcgR, responds to the elevated c-di-GMP concentration to regulate bacterial motility and then is involved in biofilm formation by facilitating the subsequent surface attachment (4, 7, 11, 12). The increased concentration of c-di-GMP activates YcgR to impair motility upon knockout of the PDE gene *yhjH* (Δ*yhjH*), whereas the inhibition of motility can be substantially rescued by deletion of the gene *ycgR* (Δ*yhjH*Δ*ycgR*) (8, 13). The swimming behavior of *E. coli* and related bacteria relies on simulta-

This work was supported by National Natural Science Foundation of China Grants 31700661 (to Y.-J. H.) and 31270792 (to D.-F. L.), Ministry of Science and Technology of the People's Republic of China Grants 2013CB911501 (to D.-F. L.) and 2017YFA0504000 (to D.-C. W.), Strategic Priority Research Program of the Chinese Academy of Sciences Grant XDB08020202 (to D.-C. W.), and the program Youth Innovation Promotion Association of the Chinese Academy of Sciences Grant 2014079 (to D.-F. L.). The authors declare that they have no conflicts of interest with the contents of this article.

This article contains Tables S1 and S2 and Figs. S1–S7.

The atomic coordinates and structure factors (codes 5Y6F, 5Y6G, and 5Y6H) have been deposited in the Protein Data Bank (http://wwpdb.org/).

The SAXS data and structural models have been deposited at SASBDB with accession numbers SASDEB9 and SASDEC9.

[1] To whom correspondence may be addressed: National Laboratory of Biomacromolecules, CAS Center for Excellence in Biomacromolecules, Institute of Biophysics, Chinese Academy of Sciences, 15 Datun Rd., Beijing 100101, China. Tel.: 86-10-64888548; Fax: 86-10-64888560; E-mail: dcwang@ibp.ac.cn.

[2] To whom correspondence may be addressed: State Key Laboratory of Microbial Resources, Institute of Microbiology, Chinese Academy of Sciences, No. 1 Beichen West Rd., Beijing 100101, China. Tel.: 86-10-64807581; Fax: 86-10-64888560; E-mail: lidefeng@im.ac.cn.

[3] The abbreviations used are: c-di-GMP/cdG, cyclic-di-GMP; DGC, diguanylate cyclase; PDE, phosphodiesterase; CCW, counterclockwise; CW, clockwise; MotAc, cytoplasmic part of MotA; FliMN, the complex of FliM and FliN; SEC, size-exclusion chromatography; AUC, analytical ultracentrifuge; SAXS, small-angle X-ray scattering; mAu, milliabsorbance units; Ni-NTA, nickel-nitrilotriacetic acid; SeMet, selenomethionine; D_{max}, maximum dimension; QDN/AAA, YcgR triple-mutant Q38A/D54A/N62A; SUMO, small ubiquitin-like modifier; ITC, isothermal titration calorimetry; LB, Luria–Bertani; IPTG, isopropyl 1-thio-β-D-galactopyranoside; BisTris, 2-[bis(2-hydroxyethyl)-amino]-2-(hydroxymethyl)propane-1,3-diol; HA, hemagglutinin.

neous flagellar counterclockwise (CCW) rotation forming the bundle, whereas clockwise (CW) rotation induces the cells to tumble upon bundle disassembly (14). This flagellar rotation is driven by a motor, which consists of at least 11 stators across the inner membrane (15), with four copies of MotA and two copies of MotB in each stator (16), along with a rotor at the bottom of the basal body, containing ~26 FliG proteins, 34 FliM proteins, and over 100 FliN proteins (17). The electrostatic interactions between the cytoplasmic domain of MotA and the C-terminal domain of FliG convert the chemical energy that is produced by the proton flow across the integral membrane channels of the stator into torque to drive the flagellar rotation (18). The flagellar rotation can be regulated via some regulators interacting with rotor proteins, such as phosphorylated CheY that binds to FliM and FliN to switch CCW rotation to CW in *E. coli* and *Salmonella typhimurium* (19, 20) and EspE that binds to FliG as a clutch during biofilm formation in *Bacillus subtilis* (21, 22). In contrast, YcgR is proposed to directly interact with different targets, the stator protein MotA or the rotor proteins FliG and FliM, in a brakelike fashion upon c-di-GMP binding by independent studies (7, 11, 12).

Boehm *et al.* (7) suggested that YcgR binds to MotA in flagellar basal bodies based on FRET assay in living cells. The FRET signal between fluorescently labeled MotA and YcgR is strong in the presence of high c-di-GMP concentration and weak in the low c-di-GMP concentration, suggesting that the MotA-YcgR interaction correlates with the cellular c-di-GMP concentration (7). They proposed that YcgR interacts with MotA at the MotA-FliG interface, thus interfering the MotA-FliG interaction and slowing down bacterial swimming velocity in a c-di-GMP-dependent manner (7). Paul *et al.* (11) identified that YcgR could pull down FliG and FliM in crude *E. coli* extracts. They observed that the mutation of residues in YcgR-N domain (N62W and K81D) weakened the binding ability of YcgR to FliG, not that to FliM, and that the mutation of residues in the PilZ domain (Q223P and I227W) weakened the binding ability to FliM, not FliG, and concluded that YcgR interacts with FliG and FliM via its YcgR-N and PilZ domains, respectively (11). They thus proposed a model that YcgR reduces the efficiency of torque generation and biases the flagella rotation by interacting with both FliG and FliM (11). Meanwhile, they did not rule out the MotA-YcgR interaction and actually proposed a potential MotA-YcgR interaction weaker than the binding of YcgR to FliG and FliM (11). Fang and Gomelsky (12) showed YcgR interaction with FliG based on pulldown and two-hybrid assays. They also observed an interaction of YcgR with FliM in two-hybrid assays only when YcgR variant R118D was the partner pair. They proposed that YcgR binds to the central fragment of FliG where FliM binds, thus altering FliG-FliM interaction and biasing the flagella rotation (12). These studies make a great improvement for the knowledge of c-di-GMP regulating flagellar motility. However, these different target proteins do not complete the puzzle of YcgR-mediated motility regulation, and where and how YcgR binds to the motor still needs more investigation to clarify (23, 24).

Previously, we undertook the crystallization and preliminary crystallographic analysis of *E. coli* YcgR in complex with c-di-GMP (25). Here, we find that YcgR could interact with the stator protein MotA *in vitro*. We determine the crystal structure of YcgR from *E. coli* in complex with its ligand, c-di-GMP, and provide direct evidence that c-di-GMP activates YcgR to bind to MotA at the MotA-FliG interface via a MotA-interacting patch formed by residue Phe^{117} in R*XXX*R motif and the C-tail helix α3 (residues 218–240) in the PilZ domain. We also demonstrate that some conserved residues in the YcgR-N domain, which is independent of MotA binding, are required for motility regulation. Thus, we discuss how c-di-GMP–activated YcgR regulates the flagellar motility via motor proteins. Further, the interaction mode between YcgR and motor proteins could be shared by other PilZ family proteins acting on their targets.

Results

YcgR stably binds to MotA with a molecular ratio of 1:4 in a c-di-GMP–dependent manner

To clarify the specific target(s) to which activated YcgR binds, we tested the interactions between YcgR and flagellar motor proteins of *E. coli* using analytical size-exclusion chromatography (SEC). The soluble cytoplasmic part of MotA (MotAc, residues 70–170) was used in the assay, because MotA is a membrane-spanning protein (26, 27). In the presence of ligand-free YcgR, MotAc was eluted at a volume of 13.71 ml, corresponding to an apparent molecular weight of 63.4 kDa and suggesting a MotAc tetramer in solution that is in line with the previously reported tetramers of full-length MotA and its transmembrane domain (16, 28) (Fig. 1*A*). YcgR was eluted at a volume of 15.07 ml with an apparent molecular weight of 33.5 kDa (Fig. 1*A*). Both of them were eluted with elution volumes and apparent molecular weights similar to those of the individual proteins (Fig. S1). With the c-di-GMP–bound YcgR, MotAc was eluted at a volume of 12.87 ml, corresponding to an apparent molecular weight of 94.1 kDa and suggesting a MotAc tetramer bound to a single ligand-bound YcgR monomer with an apparent molecular weight of 30.9 kDa (Fig. 1*B*). Subsequent analysis using an SDS-PAGE assay and the relatively high absorbance at 254 nm (A_{254}) confirmed that the eluted MotAc was accompanied by both YcgR and c-di-GMP (Fig. 1*B*). In contrast, neither FliG nor the complex of FliM and FliN (FliMN) could be eluted together with c-di-GMP–free or –bound YcgR (Fig. S2), suggesting that the recombinant FliG and FliMN could not form a stable complex with either YcgR form in the SEC assay.

The molecular weights of those protein samples have also been assayed using an analytic analytical ultracentrifuge (AUC). The results of AUC assays indicated a molecular weight of 30.7 kDa for c-di-GMP-bound YcgR (Fig. 1*C*), a monomer in line with the result of the SEC assay (Fig. S1). The result of MotAc showed two peaks, 22.3 and 54.4 kDa (Fig. 1*C*), implying a dimer-tetramer equilibration different from that observed in the SEC assay. The result of the MotAc-YcgR-c-di-GMP complex showed three peaks, 19.4, 33.1, and 86.7 kDa (Fig. 1*C*), suggesting the existence of MotAc dimer, YcgR-c-di-GMP, and the complex of MotAc tetramer and YcgR. These results indicated that MotAc could interact with YcgR-c-di-GMP.

To further obtain overall information of the complex of MotAc-YcgR-c-di-GMP, we performed small angle X-ray scat-

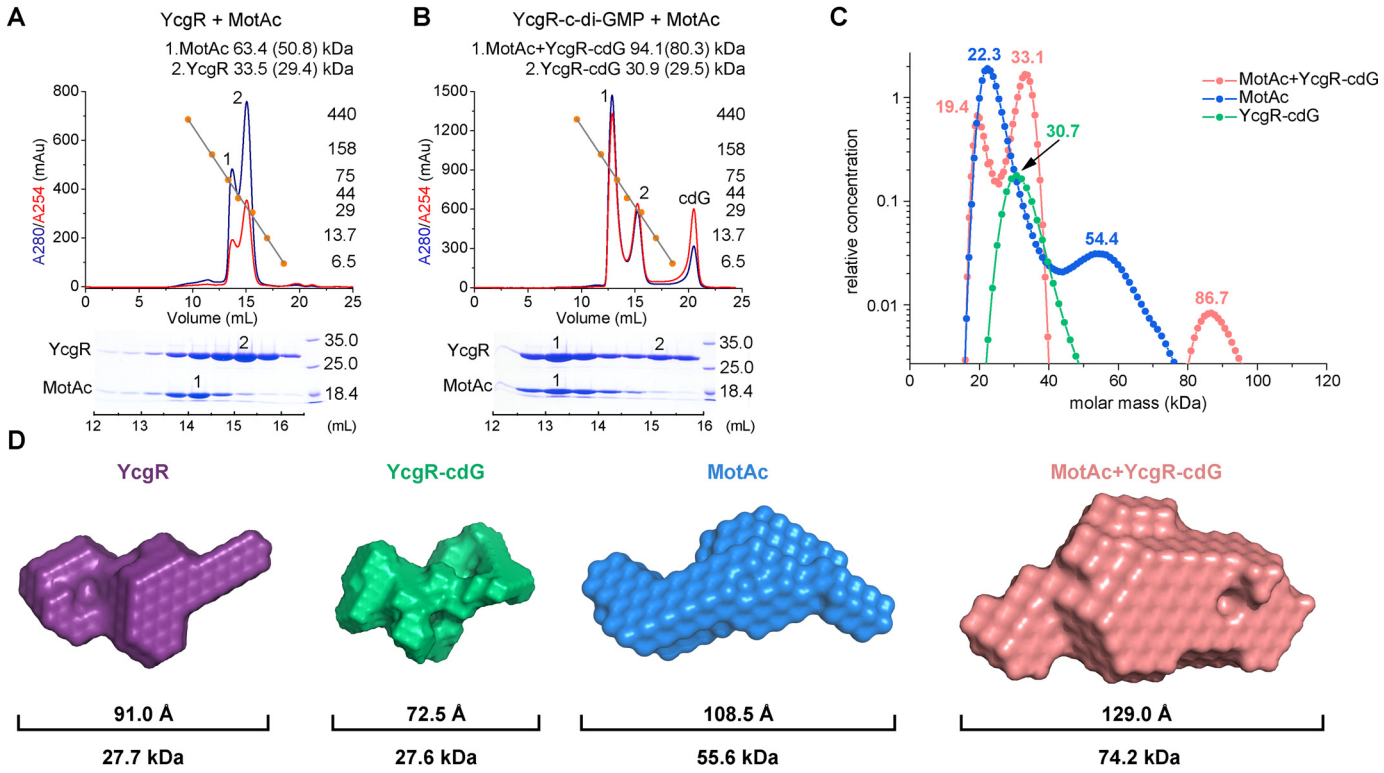

Figure 1. YcgR binds to MotA in a c-di-GMP–dependent manner. *A*, SEC assay of MotAc with YcgR. Ferritin, aldolase, conalbumin, ovalbumin, carbonic anhydrase, RNase, and aprotinin were used to measure the apparent molecular masses, shown as *orange dots* and *labeled* with their molecular weights (440–6.5 kDa) on the *right*. The calculated molecular masses are shown in *parentheses*. The SEC fractions were analyzed by SDS-PAGE and visualized by Coomassie staining at the *bottom* of the chromatogram. The *lines below* the SDS-polyacrylamide gel represent the elution volumes of fractions. Protein markers are *labeled* with their molecular weights to the *right* of the *lanes* (18.4–35.0 kDa). *B*, SEC assay of MotAc with c-di-GMP (*cdG* in the *graph*) bound YcgR. *C*, analytical ultracentrifugation assay of YcgR-c-di-GMP, MotAc, and the complex of MotAc and YcgR-c-di-GMP. *D*, *ab initio* SAXS models reconstructed by DAMMIF (29) for YcgR, YcgR-cdG, MotAc, and the complex of MotAc and YcgR-c-di-GMP. The maximum particle dimension (D_{max}) of them obtained using distance distribution functions ($P(r)$) (Fig. S3) and the molecular weight of each model calculated from the SAXS data are shown *below* the models.

tering assays (SAXS). The molecular masses of the proteins were calculated through Guinier analysis based on the scattering intensity extrapolated to zero angle ($I(0)$). All of them (YcgR, 27.7 kDa; YcgR-c-di-GMP, 27.6 kDa; MotAc, 55.6 kDa; MotAc-YcgR-c-id-GMP, 74.2 kDa) (Fig. 1*D*) were similar to those estimated by analytical SEC and AUC. The maximum dimension D_{max} of each sample was obtained using the pair distance distribution function $P(r)$ (Fig. 1*D* and Fig. S3). The *ab initio* model of YcgR, YcgR-ci-GMP, MotAc, and the complex of MotAc and YcgR-c-di-GMP were built using DAMMIF (29) (Fig. 1*D* and Fig. S3). These results further corroborate that YcgR binds to MotAc in a c-di-GMP–dependent manner.

c-di-GMP binding is essential for YcgR interacting with MotA and regulating motility

In view of the low sequence identities between YcgR from *E. coli* and other PilZ domain–containing proteins whose structures have been determined (*i.e.* 18.22% for PP4397 from *Pseudomonas putida* (30), 16.40% for MrkH from *Klebsiella pneumoniae* (31, 32), and 15.42% for MotI from *Bacillus subtilis* (33)), we determined the crystal structure of YcgR-c-di-GMP complex from *E. coli* at a resolution of 2.30 Å (data collection and refinement statistics given in Table S1) to investigate the mechanism of c-di-GMP regulating the binding ability of YcgR to the motor. The structure indicated that YcgR folds into two individual domains, an N-terminal YcgR-N domain and a C-terminal PilZ domain (Fig. 2*A* and Fig. S4), similar to that observed in the structures of the homologs PP4397 (30), MrkH (31, 32), and MotI (33). The YcgR-N domain (residues 1–110) possesses a β-barrel fold, formed by single five-stranded and four-stranded anti-parallel β-sheets and clamped by two helices, α1 and α2, across the top and bottom (Fig. 2*A*). The PilZ domain (residues 111–244) shares a similar β-barrel fold, with only a helix α3 (C-tail helix) situated over the top (Fig. 2*A*). This domain contains two conserved c-di-GMP binding motifs, ^{114}R*XXX*R^{118} and ^{145}(D/N)*XSXX*G^{150}, comparable with other PilZ domains (10). The two β-barrels are bridged by a loop comprising residues 111–119, which contains the conserved motif R*XXX*R. Two mutually intercalated c-di-GMP molecules bind to this loop as well as the (D/N)*XSXX*G motif and fit into the groove formed by the two domains (Fig. 2*A*).

The structure showed that residues Arg^{113}, Arg^{114}, Arg^{118}, Asp^{145}, Ser^{147}, Arg^{208}, Ser^{190}, and Ser^{210} are involved in a hydrogen bond network to bind c-di-GMP (Fig. 2*B*). The roles of them were assessed using mutagenesis experiments. The c-di-GMP affinity of YcgR was determined using an isothermal titration calorimetry (ITC) assay, with a disassociation constant K_d of 0.141 μM and a stoichiometric ratio of 2 (Fig. 2*C* and Fig. S5*A*). Mutants R114A, R118A, and D145A retained very limited c-di-GMP affinity (Fig. 2*C* and Fig. S5*A*), did not inhibit bacterial motility (Fig. 2*D*), and did not bind to MotAc in the analyt-

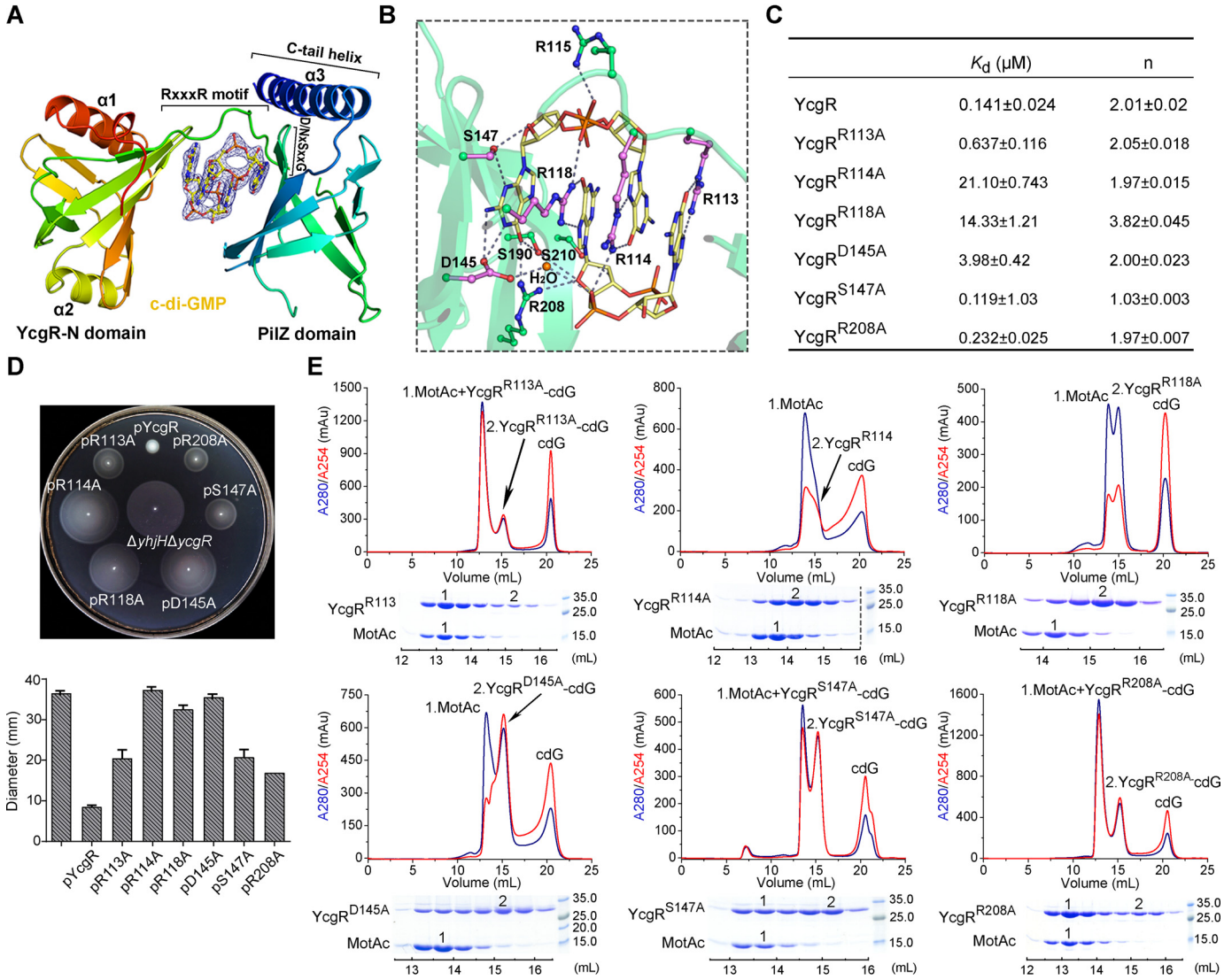

	K_d (μM)	n
YcgR	0.141±0.024	2.01±0.02
YcgR^{R113A}	0.637±0.116	2.05±0.018
YcgR^{R114A}	21.10±0.743	1.97±0.015
YcgR^{R118A}	14.33±1.21	3.82±0.045
YcgR^{D145A}	3.98±0.42	2.00±0.023
YcgR^{S147A}	0.119±1.03	1.03±0.003
YcgR^{R208A}	0.232±0.025	1.97±0.007

Figure 2. Essential roles of c-di-GMP–binding residues in bacterial motility and MotA interaction. *A*, *cartoon representation* of the YcgR-c-di-GMP complex structure. The ligand in a *ball-and-stick model* is surrounded by a ligand-omitted $F_o - F_c$ electron density map contoured at 3 δ (*blue*). *B*, the binding details of c-di-GMP. The side chains of conserved residues involved in the hydrogen bond network are shown in *violet*, and the others are shown in *green*. The hydrogen bonds are shown as *dark gray dashes*. *C*, statistics list of binding parameters of c-di-GMP and its binding residue mutants of YcgR measured by ITC. *D*, motility assay of strains harboring YcgR mutants involved in c-di-GMP binding. Mutants fused to C-terminal HA tags were expressed from plasmids in the *ΔyhjHΔycgR* strain, and the expressions were detected using anti-HA antibody (Fig. S6*A*). The histogram depicts the mean and *error bars* representing S.D. from five independent tests. *E*, SEC assay showing the interactions between YcgR mutants and MotAc in the presence of c-di-GMP (*cdG* in the *graph*). The elution fractions were analyzed by Coomassie-stained SDS-PAGE, shown at the *bottom* of corresponding chromatographic plots. The *lines below* the SDS-polyacrylamide gel represent the elution volumes of fractions.

ical SEC assay (Fig. 2*E*). Notably, a previous study reported that c-di-GMP levels caused by the yhjH deletion were not enough for the binding of BcsA, which binds c-di-GMP with a K_d of 8.2 μM, to trigger cellulose production (3). We therefore suggested that the c-di-GMP concentration in strain Δ*yhjH* could not activate those YcgR mutants, because they maintained similar c-di-GMP affinities to BcsA (R114A with K_d of 21.1 μM, R118A with K_d of 14.33 μM, and D145A with K_d of 3.98 μM; Fig. S5*A*). Mutants R113A and R208A maintained low c-di-GMP affinity (Fig. 2*C* and Fig. S5*A*) and approximately half of the motility inhibition ability compared with the WT (Fig. 2*D*), although they were observed to bind to MotAc in the SEC assay with elution plots similar to that of the WT (Fig. 2*E*). These results suggest that the loss or decrease of c-di-GMP affinity for YcgR leads to the loss or decrease of its ability to interact with MotA and inhibit the motility. Mutant S147A retained a somewhat high c-di-GMP affinity (Fig. 2*C* and Fig. S5*A*) and still bound to MotAc (Fig. 2*E*), yet only exhibited a fraction of the motility inhibition ability (Fig. 2*D*). It is possible that the mutation decreased the stability of YcgR and then impaired the motility. Meanwhile, considering that only a single c-di-GMP binds to S147A (Fig. 2*C* and Fig. S5*A*) and that the mutation confers a SEC profile different from that of WT YcgR, we believe that the c-di-GMP dimer binding to YcgR is necessary for maintaining a proper MotAc-binding region and then for motility regulation. Therefore, we conclude that the c-di-GMP binding is essential for YcgR interaction with MotA and regulation of the motility and that the conserved residues Arg^{113}, Arg^{114}, Arg^{118}, Asp^{145}, and Ser^{147} preferentially function in c-di-GMP recognition rather than MotA interaction.

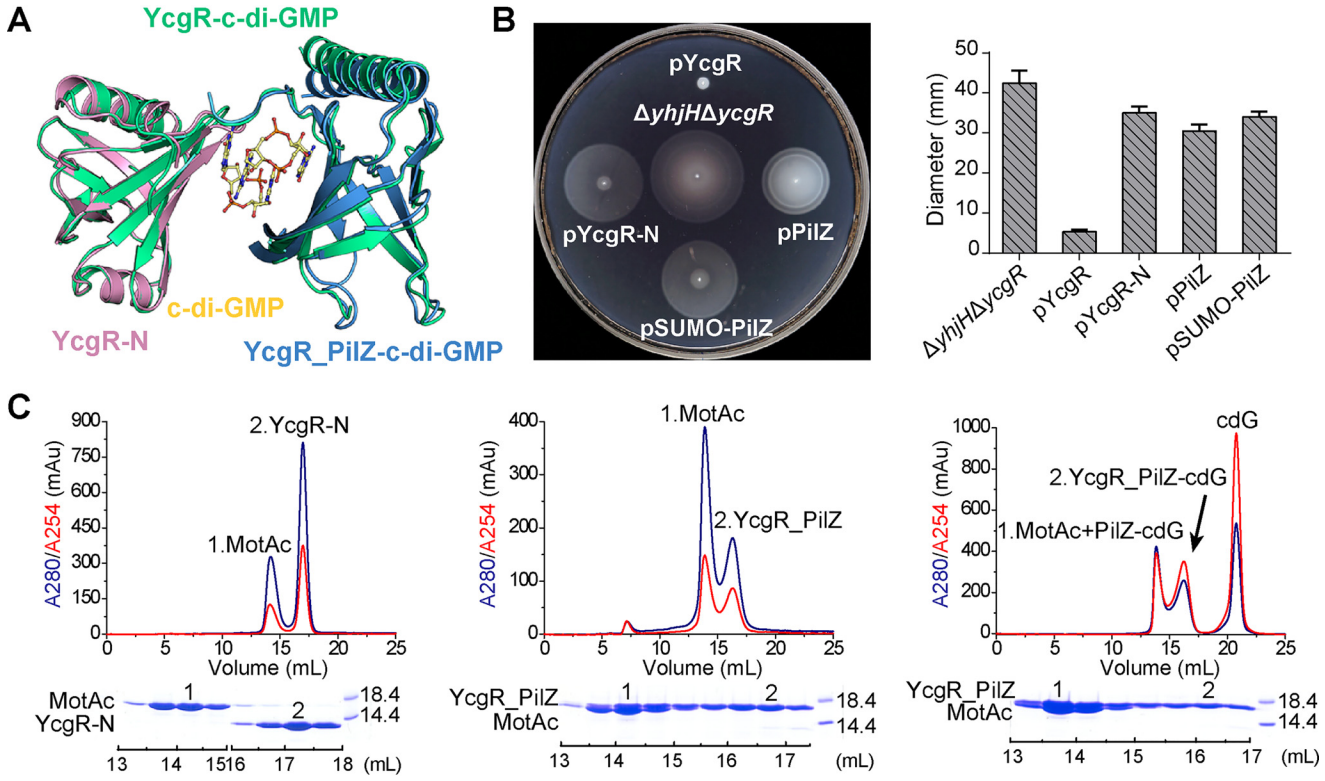

Figure 3. Both YcgR-N and PilZ domains are requisite for motility regulation. *A*, superposition of the structures of c-di-GMP-bound YcgR (*green*), the YcgR-N domain (*pink*), and the PilZ domain in complex with c-di-GMP (*blue*). *B*, motility assay of strains harboring individual YcgR-N domains, PilZ domains, and PilZ with an N-terminal SUMO tag (as a control). All of them were fused with a C-terminal HA tag and expressed by plasmids in the Δ*yhjH*Δ*ycgR* strain, and the expressions were detected using anti-HA antibody shown in Fig. S6*B*. The histogram depicts the mean and *error bars* representing S.D. from five independent tests. *C*, SEC assay of the MotAc-interacting ability of YcgR-N (*left*) and c-di-GMP (*cdG*)-free (*middle*) and -bound (*right*) PilZ domains. The elution fractions were analyzed by Coomassie-stained SDS-PAGE, shown at the *bottom* of corresponding chromatographic plots. The *lines* below the SDS-polyacrylamide gel represent the elution volumes of fractions.

An individual PilZ domain is sufficient to interact with MotA upon c-di-GMP binding, whereas both YcgR-N and PilZ domains are requisite for motility regulation

To unravel the roles of the YcgR-N and PilZ domains in the YcgR-MotA interaction pattern, we obtained both the crystal structure of individual YcgR-N and that of PilZ in complex with c-di-GMP (data collection and refinement statistics given in Table S1). These structures are almost identical to those of the two domains in the YcgR-c-di-GMP structure (Fig. 3*A*), suggesting that the YcgR-N domain would not undertake a significant conformational change upon the binding of c-di-GMP. The roles of the individual YcgR-N and PilZ domains were assessed using the c-di-GMP–binding, MotAc-interacting, and bacterial motility assays. The YcgR-N domain did not bind c-di-GMP *in vitro* and did not form a stable complex with MotAc in the SEC assay (Fig. S5*B* and Fig. 3*C*). Conversely, the PilZ domain bound c-di-GMP, as reported previously (8), with somewhat higher affinity (K_d of 0.099 μM) than YcgR (Fig. S5*B*). Notably, it could bind to MotAc upon c-di-GMP binding (Fig. 3*C*). Nevertheless, neither domain could restore the motility inhibition ability of YcgR (Fig. 3*B*). These results clearly indicate that MotA binding is not sufficient for the motility inhibition and that both YcgR-N and PilZ domains are required for motility regulation.

c-di-GMP binding induces the RXXXR motif and the C-tail helix to form a MotA-interacting patch

To identify which residues directly participate in the interaction between YcgR and MotA, we performed multiple-sequence alignment and found two conserved regions in the PilZ domain including residues Gln^{112} and Phe^{117} in the R*XXX*R motif and residues Glu^{221}, Arg^{222}, Gln^{225}, Arg^{226}, Ile^{228}, Phe^{229}, Glu^{232}, and Glu^{234} in the C-tail helix (Fig. 4*A*). To reveal the local conformational change of these residues induced by c-di-GMP, we attempted to solve the ligand-free structure; however, this was not successful. Thus, we studied the global conformational change using SAXS assay (Fig. 4*B*) and built a ligand-free rigid-body model (Fig. S4*B*). Superposition of the ligand-bound and -free models shows a large-scale domain movement (Fig. 4*C*), which has been also observed in YcgR homologs (30, 34). A close inspection indicated that c-di-GMP anchors the side chains of Arg^{113}, Arg^{114}, Arg^{115}, and Arg^{118} (Fig. 4*C*, *pink box*), exposes the side chain of Phe^{117}, and triggers a rearrangement of the R*XXX*R motif and the C-tail helix α3 to form a potential binding region for partners (Fig. 4*C*, *blue box*). These residues were then examined using mutagenesis experiments to assay their roles in c-di-GMP affinity, MotA-interacting ability, and motility regulation.

Mutant F117A presented somewhat high affinity to c-di-GMP (Fig. S5*C*) but lost the ability to interact with MotA and

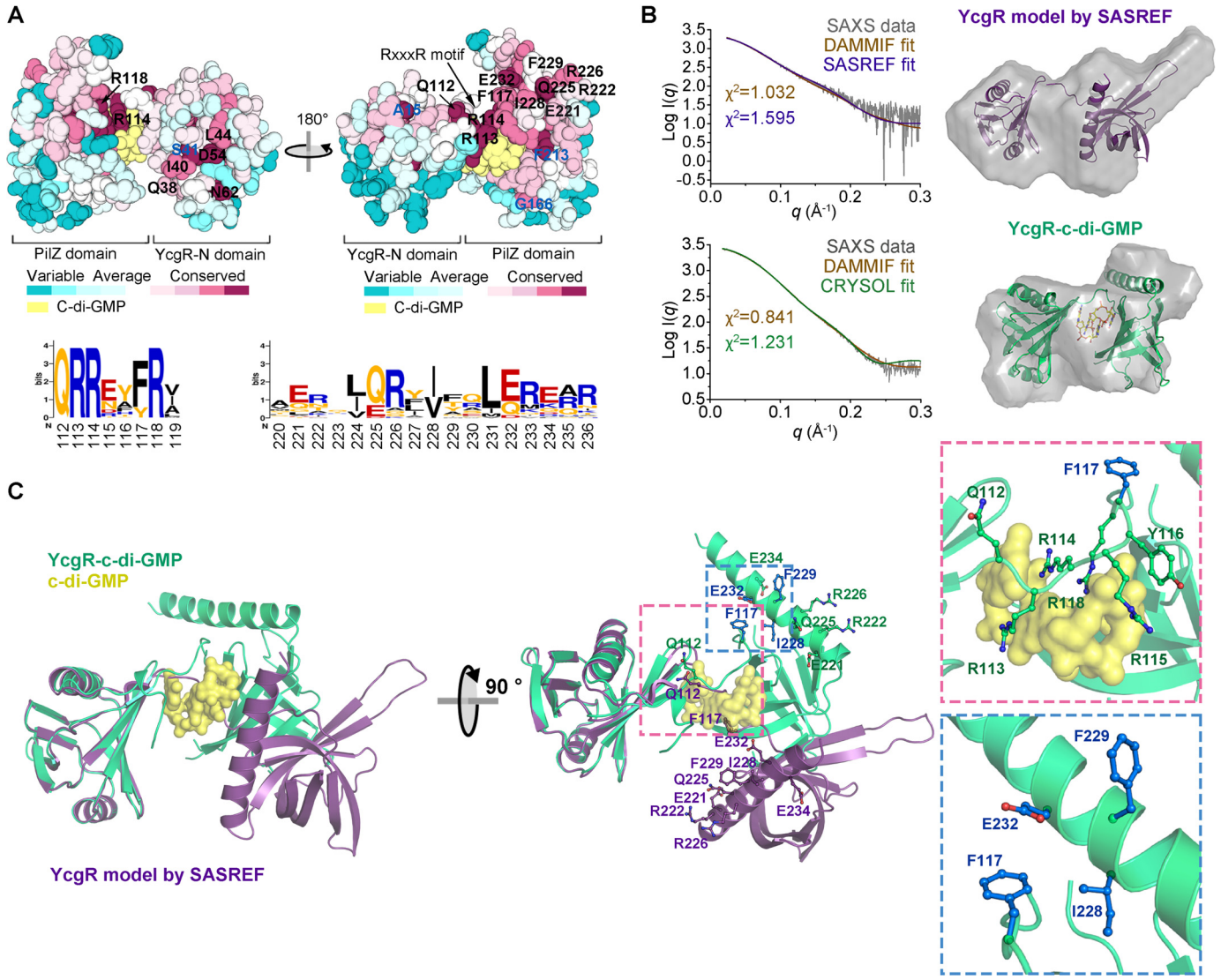

Figure 4. c-di-GMP induces the rearrangement of YcgR domains. *A*, distribution of conserved residues generated by ConSurf Server (54). The conserved residues are *labeled*, among which the buried residues are marked in *blue*. The sequence consensus of R*XXX*R motif and C-tail helix are shown using "Weblogo" (55) at the *bottom*. The *residue numbers below* the "Weblogo" are according to YcgR from *E. coli*. The acidic, basic, nonpolar, and polar residues are shown in *red*, *blue*, *black*, and *yellow*, respectively. *B*, SXAS assay of YcgR and YcgR-c-di-GMP. In the *left panel*, the experimental spectra of SAXS data are shown in *gray*. The shape reconstruction of YcgR and YcgR-c-di-GMP by DAMMIF (29) (*brown*) show good agreement with the theoretical data calculated from the YcgR model constructed by SASREF (*purple*) and the crystal structure of YcgR-c-di-GMP (*green*). In the *right panel*, the most probable envelope (*gray*) of ligand-free/bound YcgR predicted by DAMMIF was superimposed with the YcgR model and the structure of YcgR-c-di-GMP. *C*, superposition of the c-di-GMP-bound crystal structure (*green*) and the ligand-free model built by SASREF (*purple*). The residues in and around the R*XXX*R motif are *boxed* in *pink dotted lines*, and the residues involved in the MotA-interacting patch are *boxed* in *blue dotted lines*. The residues forming the MotA-interacting patch are *highlighted* in *blue*.

inhibit motility (Fig. 5, *A* and *B*), revealing that Phe^{117} is directly involved in the MotA interaction, which is essential for motility regulation. Mutant Q112A maintained the c-di-GMP affinity (Fig. S5*C*) and interacted with MotAc (Fig. 5*B*). However, it lost the majority of its motility inhibition ability (Fig. 5*A*), possibly because Gln^{112} is close to the YcgR-MotA interface. The roles of conserved residues Glu^{221}, Arg^{222}, Gln^{225}, Arg^{226}, Ile^{228}, Phe^{229}, Glu^{232}, and Glu^{234} in the C-tail helix were subsequently checked. The substitution of residues at the immediate vicinity of Phe^{117} (Fig. 4*C*), residues Ile^{228}, Phe^{229}, or Glu^{232}, to alanine abolished the bacterial motility inhibition function of YcgR, whereas the substitution of the other residues did not (Fig. 5*A*). In addition, mutants I228A, F229A, and E232A also abolished the MotAc-binding ability and maintained the c-di-GMP affinity (Fig. 5*B* and Fig. S5*C*), indicating that these three residues, similar to Phe^{117}, are directly involved in the interaction with MotA and subsequently in mobility inhibition. These findings demonstrate that residue Phe^{117} in the ligand binding motif R*XXX*R and residues Ile^{228}, Phe^{229}, and Glu^{232} in the C-tail helix form a MotA interacting patch upon c-di-GMP binding, and this patch is essential for YcgR-MotA interaction and motility regulation.

The YcgR interacting site of MotA was consequently investigated. It has been reported that the YcgR-interacting site is in or close to the MotA-FliG interface (residues Arg^{90}–Glu^{98} of MotA) and includes residues Gly^{93} and Ser^{96} (7). However, the mutations of those MotA suppressors (*e.g.* G93R and S96L) resulted in the aggregation of MotAc. A mutagenesis scanning of the MotA-FliG interface (*i.e.* residues Arg^{90}–Glu^{98}) was performed. The SEC assay indicated that mutants R90A, M92A,

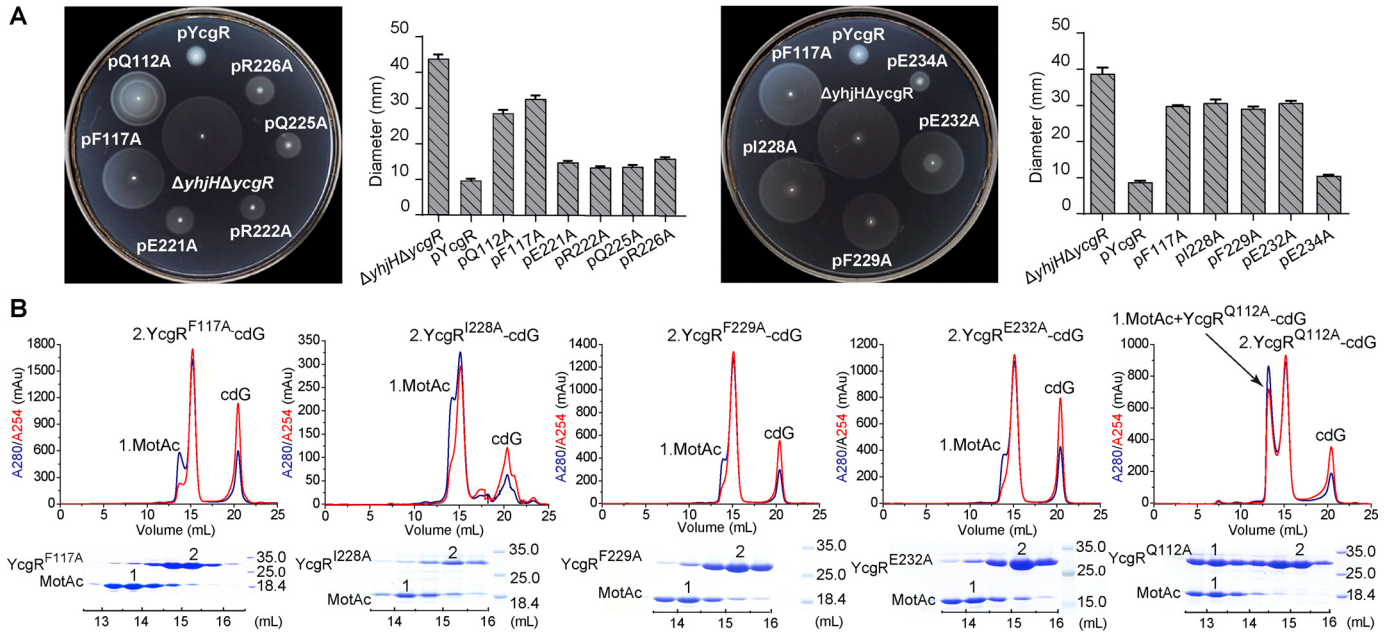

Figure 5. Conserved R*XXX*R motif and the C-tail helix constitute the MotA-interacting patch. *A*, motility assay of strains harboring YcgR mutants (fused to a C-terminal HA tag) involved in the MotA-interacting patch. The expressions of mutants were detected using anti-HA antibody and shown in Fig. S6*C*. The histogram depicts the mean and *error bars* representing S.D. from five independent tests as shown to the *right* of the plates. *B*, MotAc-interacting ability of c-di-GMP (*cdG*)-bound YcgR mutants assayed by SEC. The elution fractions were analyzed by Coomassie-stained SDS-PAGE, shown at the *bottom* of corresponding chromatographic plots. The *lines below* the SDS-polyacrylamide gel represent the elution volumes of fractions.

G93A, M94A, F95A, and E98A lost their YcgR-binding abilities (Fig. 6), whereas Q91A and S96A remained (Fig. 6). Taken together, YcgR is activated by c-di-GMP to tightly interact with MotA at MotA-FliG interface via the patch consisting of R*XXX*R motif and C-tail helix in the PilZ domain.

A conserved region of the YcgR-N domain is necessary for regulating motility

The previous results confirmed that both the YcgR-N and PilZ domains are essential for motility regulation. We investigated the possible role of YcgR-N and key residues involved in motility regulation. Sequence alignment of YcgR similarities revealed residues Gln^{38}, Ile^{40}, Leu^{44}, Asp^{54}, and Asn^{62} as conserved (Fig. 4*A*). In the structure, they are located at the same side of the YcgR-N β-barrel, distant from the MotA-binding patch (Fig. 7*A*). The substitution of residue Gln^{38}, Ile^{40}, Leu^{44}, Asp^{54}, or Asn^{62} to alanine decreased the mobility inhibition ability (Fig. 7*B*), implying their roles in motility regulation. In comparison, the triple-mutant Q38A/D54A/N62A (QDN/AAA) displayed lower motility inhibition ability than the single mutants (Fig. 7*B*), but retained the same c-di-GMP affinity (Fig. S5*D*) and MotA interacting ability as the WT (Fig. 7*C*), revealing that these residues are independent from c-di-GMP and MotA binding. The results suggest that these residues may be involved in interactions with other proteins (*e.g.* the rotor proteins FliG and FliM described in previous research (11, 12)) and then regulation of flagella rotation.

Discussion

Cellular levels of c-di-GMP are related to controlling the transition of bacteria from motile to sessile. YcgR, as a PilZ-containing protein in *E. coli* and related species, responds to the elevated c-di-GMP concentration by reducing the flagella motor output, slowing down the swimming velocity in a brake-like fashion and facilitating bacterial surface attachment and subsequent biofilm formation (4). Previously, three independent studies suggested the motor proteins MotA, FliG, and FliM as the YcgR partners (7, 11, 12). These studies proposed different models where YcgR interacted with different targets (*i.e.* MotA (7), both FliG and FliM (11), or individual FliG (12)) to regulate motility and suggested that activated YcgR alters the MotA-FliG (7, 11) or FliG-FliM (12) interaction to decrease the flagellar rotation speed and induce CCW motor bias. These observations suggest that YcgR possibly interacts with multiple proteins within the motor to control the motor output and bias flagellum rotation. Here, we provide novel evidence that both the YcgR-N and PilZ domains are necessary for c-di-GMP regulating flagellar motility. We identify that YcgR could interact with the stator protein MotA via its PilZ domain and propose that a conserved region formed by Gln^{38}, Ile^{40}, Leu^{44}, Asp^{54}, and Asn^{62} in the YcgR-N domain contributes to the interaction with some other motor proteins.

MotA is proposed as the YcgR partner in the study of Boehm *et al.* (7), where c-di-GMP–activated YcgR interacts with MotA and reduces flagellar motor function in a brakelike fashion. Previous studies also reported the interaction of two MotA homologues, MotI from *B. subtilis* (33) and FlgZ from *Pseudomonas aeruginosa* (35), with MotA or a MotA homolog MotC. Our study provides direct evidence that YcgR interacts with MotA. We show that YcgR could interact with MotA via its PilZ domain to form a 1:4 complex in the presence of c-di-GMP (Fig. 1*B*), suggesting that one stator complex, $MotA_4MotB_2$, only binds one YcgR molecule. We determined the crystal structure of YcgR-c-di-GMP complex (Fig. 2*A*). Because the ligand-free YcgR was too difficult to crystallize, we proposed a ligand-free

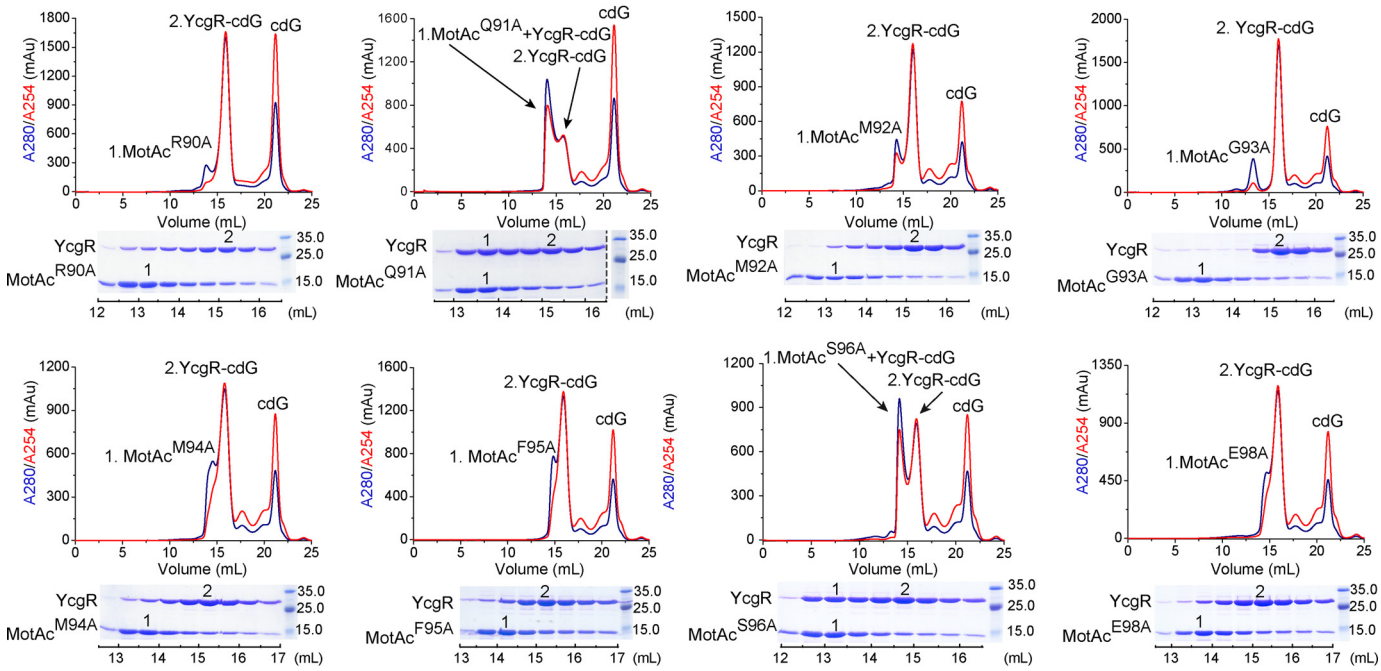

Figure 6. MotA interacts with YcgR via the MotA-FliG interface. The binding abilities between MotAc mutants involved in MotA-FliG interface and YcgR in the presence of c-di-GMP are detected by an SEC assay. The elution fractions were analyzed by Coomassie-stained SDS-PAGE, shown at the *bottom* of corresponding chromatographic plots. The *lines below* the SDS-polyacrylamide gel represent the elution volumes of fractions.

YcgR model using a SAXS assay based on the crystal structure of YcgR-N domain and the homology model of ligand-free PilZ domain (Fig. 4*B*). Our structural and SEC assays indicate that c-di-GMP binding induces the R*XXX*R motif and C-tail helix to form a MotA-interacting patch (Fig. 4*C*). The residues Phe^{117}, Ile^{228}, Phe^{229}, and Glu^{232} that constitute the patch are conserved across different bacteria (Fig. 4*A* and Fig. S4), suggesting that YcgR similarities share a common mode of c-di-GMP-activated interaction with MotA. Meanwhile, we identify that residues Arg^{90}, Met^{92}, Gly^{93}, Met^{94}, Phe^{95}, and Glu^{98} of MotA, which situate at the MotA-FliG interface, are involved in the interaction between MotA and YcgR (Fig. 6). This result is in line with the previous observation that mutation G93R of MotA impaired the YcgR inhibition ability (7) and confirms that YcgR binds to MotA at the MotA-FliG interface.

However, YcgR binding to MotA at the MotA-FliG interface is not sufficient for motility regulation, supported by malfunction of individual PilZ domain (Fig. 3*B*) as well as YcgR mutants harboring the alanine substitution of conserved residues in YcgR-N domain (Fig. 7*B*). Some conserved residues in the YcgR-N domain, including Gln^{38}, Ile^{40}, Leu^{44}, Asp^{54}, and Asn^{62}, are involved in motility regulation. The triple mutation QDN/AAA impaired motility regulation ability (Fig. 7*B*) yet kept the similar affinity with c-di-GMP and still formed a stable complex with MotAc (Fig. S5*D* and Fig. 7*C*). It has been reported that the rotor proteins FliG and FliM are also the targets of YcgR (11, 12); thus, we infer that these residues consist of an interaction region for them. Residue Asn^{62} has been proposed as the interacting site for FliG (11). Therefore, we thought this conserved region in the YcgR-N domain might be responsible for FliG binding. The other reported residue involved in FliG interaction, Lys^{81} (11), actually interacted with c-di-GMP according to our structure and thus was eliminated from the FliG-interacting region. Previously, the role of YcgR in motility regulation was proposed to be conserved because YcgR similarities could be found across many proteobacteria (10, 11). Nevertheless, some YcgR similarities do not harbor these conserved residues in the YcgR-N domain, such as MotI from *firmicutes* (Fig. S7). MotI is proposed to sequester MotA from FliG via binding to MotA in a clutchlike fashion (33) and share the similar folding with YcgR, with an root mean square deviation of 4.72 Å for overall α-carbon positions. These findings suggest that YcgR in different bacteria could interact with various targets besides MotA and recruit different motility regulation mechanisms.

YcgR or its mutant R118D could interact with FliM, which has been proposed by Paul *et al.* (11) and Fang *et al.* (12). We have defined the roles of conserved motifs of YcgR (*i.e.* R*XXX*R and (D/N)*XSXX*G motifs for c-di-GMP binding, R*XXX*R motif and C-tail helix α3 for MotA binding, and the conserved region of the YcgR-N domain for FliG interacting). We did not find any structural and bioinformatic clues of residues potentially important for direct FliM binding. Fang and Gomelsky proposed that only the YcgR-R118D mutant interacts with FliM (12). Based on our structure and affinity assay, residue Arg^{118} is critical for c-di-GMP binding of YcgR; hence, its mutation presumably impairs the FliM interaction due to the loss of the c-di-GMP affinity. Thus residue Arg^{118} or its substitution does not seem to interact with FliM directly. Paul *et al.* (11) proposed that helix α3 is important for FliM binding. However, our findings show that this helix is vital in MotA binding, and the key residues, such as Ile^{227}, reported in the previous study were not assayed here because the side chain of Ile^{227} is buried at the protein interior and could not function as an exterior interacting site. The mutation of I227W possibly results in the

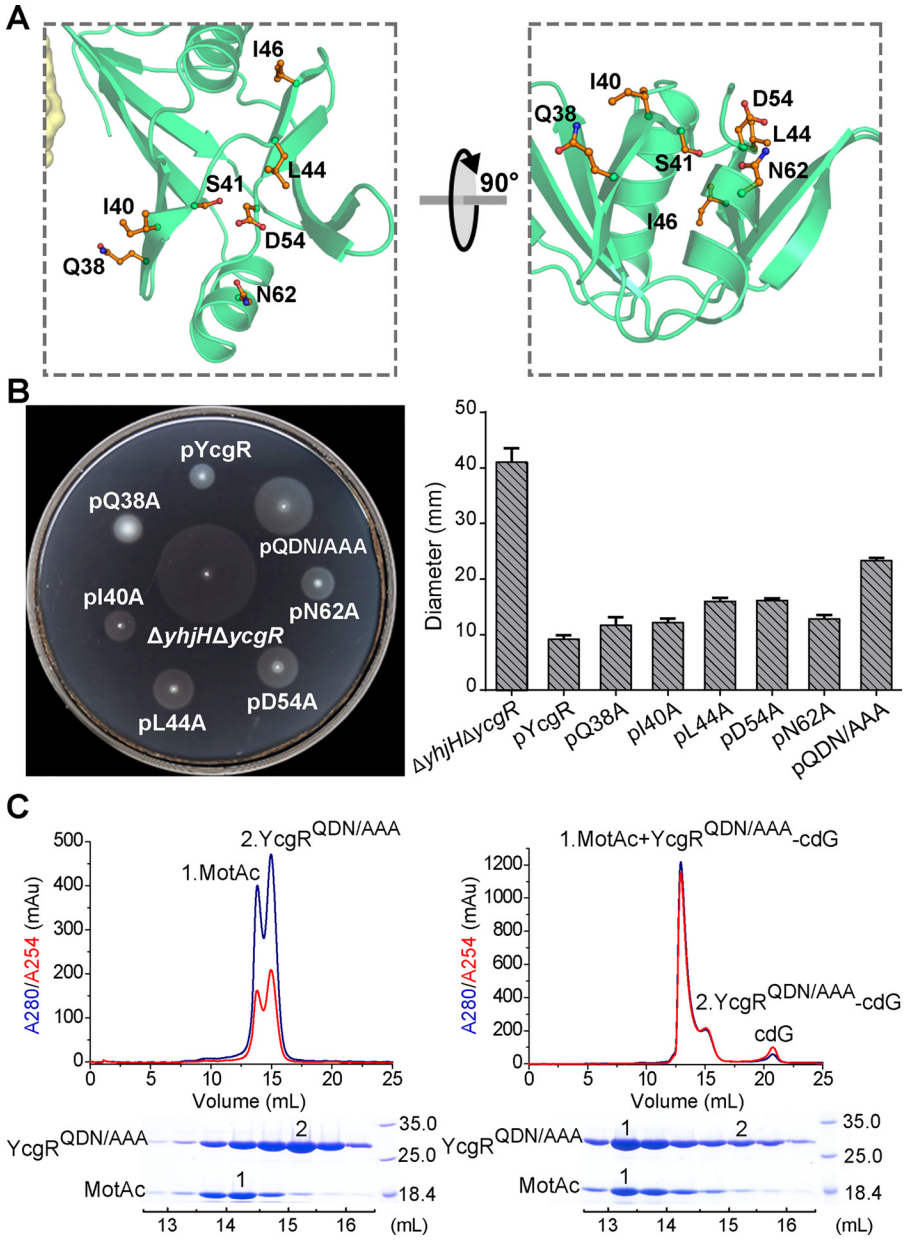

Figure 7. The conserved residues in the YcgR-N domain are required for motility regulation. *A*, detailed structural inspection of the YcgR-N conserved residues (*orange*) identified in Fig. 4*A*. *B*, bacterial motility assay of strains harboring YcgR mutants (fused to a C-terminal HA tag) involved in the conserved region of the YcgR-N domain. The expressions of the mutants *in vivo* were detected using anti-HA antibody and shown in Fig. S6*D*. The histogram depicts the mean and *error bars* representing S.D. from more than five independent tests. *C*, the MotAc-interacting ability of c-di-GMP (*cdG*)-free (*left*) and -bound (*right*) QDN/AAA assayed by SEC. The elution fractions were assayed by Coomassie-stained SDS-PAGE, as shown at the *bottom* of the chromatograms. The *lines below* the SDS-polyacrylamide gel represent the elution volumes of fractions.

improper protein fold, which could cause a low FliM (as well as MotA/FliG) affinity and a normal motor speed and bias of the strain harboring the I227W mutant (11). Thus, we could not evaluate the role of YcgR interaction with FliM. Additional experimentation will be required to explain the interaction between YcgR and FliM, along with its role in motility regulation.

Considering that both YcgR-N and PilZ domains are necessary, we propose that activated YcgR simultaneously interacts with the stator and rotor via two domains to regulate the flagellar motility. In detail, c-di-GMP binding rearranges the PilZ domain configuration to assemble a MotA-binding patch, including the R*XXX*R motif and C-tail helix α3. Activated YcgR binds to MotA at the MotA-FliG interface, which should increase the resistance and decrease energy transfer between the stator and rotor, thus slowing down bacterial swimming velocity (Fig. 8). The YcgR-N domain is inferred to interact with other motor proteins, such as FliG. Although some details still need further study to fill in, for example, how YcgR biases the flagellar rotation, our study clarified one of the key questions in YcgR-mediated motility regulation, how YcgR interacts with its target MotA. We suggest that YcgR and its similarities could interact with MotA via activated PilZ domain in a common mode and that, further, they could be involved in motility regulation via diverse mechanisms, like a brake or a clutch, depending on the YcgR-N domain. Our study paves the way for

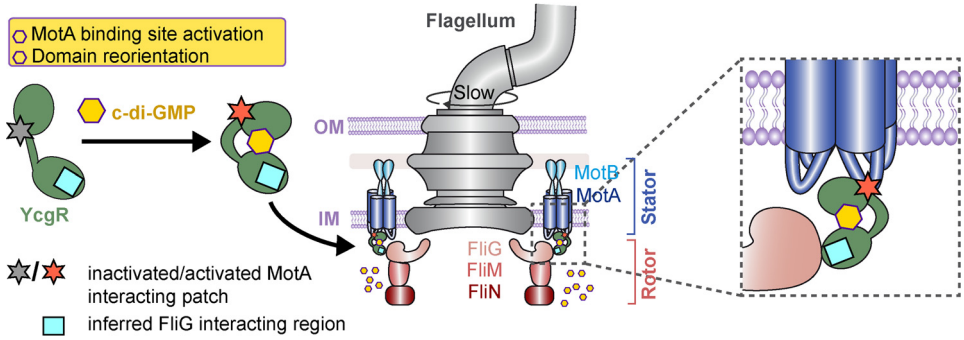

Figure 8. The proposed model of c-di-GMP regulating the YcgR-mediated flagella brake behavior. A *schematic diagram* of the bacterial flagella motor is shown. Accompanying the increased concentration of c-di-GMP, YcgR binds c-di-GMP, resulting in the activation of the MotA-binding patch and the reorientation of YcgR-N and PilZ domains. Thus, activated YcgR binds to the stator protein MotA via its PilZ domain at the MotA-FliG interface and simultaneously interacts with some motor proteins, FliG as the preferred target, via its YcgR-N domain.

further study on YcgR-mediated flagellar motility and provides new clues for investigating other PilZ proteins.

Experimental procedures

Bacterial strains and plasmids

The bacterial strains and plasmids used in this study are listed in Table S2. The genes of YcgR, FliG, FliM, and FliN were cloned from *E. coli* strain MG1655. The full-length YcgR, the N-terminal YcgR-N domain (residues 1–110), and the C-terminal PilZ domain (residues 111–244) constructs used for expression and purification were generated by subcloning in pET-22b plasmid with a His_6 tag fused to their C terminus. The sequences encoding the soluble cytoplasmic part of MotA (MotAc, residues 70–170 of MotA) and the full-length of rotor protein FliG were also cloned into the pET-22b plasmid with a C-terminal His_6 tag. Because the rotor protein FliM was inclined to aggregation in cells (36), the DNAs encoding FliM and FliN were cloned into two ORFs of co-expression plasmid pETDuet-1 with an N-terminal His_6 tag of FliM to generate FliMN. The constructs involved in motility assay were generated by subcloning in pBBR1MCS-3 (37) plasmid fused with a C-terminal HA tag. Site-directed mutants were introduced using the standard QuikChange site-directed mutagenesis kit protocol (38). The correctness of the constructs was confirmed by DNA sequencing.

Protein expression and purification

His-tagged YcgR, YcgR mutants, YcgR-N, PilZ, MotAc, FliG, and FliMN were overexpressed in *E. coli* BL21 (DE3) cells and then purified by Ni-NTA affinity chromatography and SEC. Transformed cells were cultured to A_{600} 0.8–1.0 in Luria-Bertani (LB) medium at 37 °C, and then 0.1 mM (YcgR, YcgR mutants, and PilZ) or 0.3 mM (YcgR-N, MotAc, FliG, and FliMN) IPTG was added. After another 16-h incubation at 16 °C, the cells were harvested by centrifugation. The pellets were resuspended in lysis buffer containing 20 mM Tris-HCl, pH 7.5, 300 mM NaCl, 10% glycerol, and 10 mM imidazole, lysed by sonication, and centrifuged at 4 °C for removing the cell debris. The supernatant was loaded directly onto a Ni-NTA affinity column pre-equilibrated by lysis buffer. The column was washed with wash buffer consisting of 20 mM Tris-HCl, pH 7.5, 300 mM NaCl, 10% glycerol, and 20 mM imidazole, and the target proteins were eluted with elution buffer (20 mM Tris-HCl, pH 7.5, 300 mM NaCl, 10% glycerol, and 250 mM imidazole). The eluate was concentrated and applied on a HiLoad 16/60 Superdex 75 pg (GE Healthcare) gel-filtration column equilibrated with SEC buffer (20 mM HEPES, pH 7.5, 150 mM NaCl, and 10% glycerol).

The SeMet derivative of YcgR was expressed in *E. coli* B834 (DE3) and grown in LB medium at 37 °C to an A_{600} of 1.0. The cells were harvested, resuspended in M9 minimal medium, and starved of methionine for 1 h. Then 0.25 μM SeMet (Anatrace) and 0.05 mM IPTG was added to the culture, and the cells were incubated overnight for 16 h at 16 °C. The SeMet derivative of YcgR was purified using the same buffer as above with additional 5 mM β-mercaptoethanol in Ni-NTA affinity buffer and 2 mM DTT in SEC buffer. All proteins were confirmed by SDS-PAGE, concentrated by ultrafiltration, and immediately used for crystallization or frozen and stored at −80 °C.

Analytical ultracentrifugation

Purified YcgR-c-di-GMP, MotAc, and MotAc-YcgR-c-di-GMP were concentrated to ~1 mg ml^{-1} in buffer containing 20 mM HEPES, pH 7.5, and 150 mM NaCl. An AUC assay was carried out on a Beckman Coulter Optima XL-I analytical ultracentrifuge. The experiment was performed at 20 °C at a speed of 60,000 rpm for 7 h. Raw data were processed using Sednterp, and the sedimentation coefficients and apparent molecular masses were calculated (39).

Crystallization, data collection, and structure determination

Prior to crystallization trials, purified YcgR and PilZ from *E. coli* were mixed with c-di-GMP (BioLog) at a 3:1 ligand/protein molar ratio. Crystallization was performed using the vapor diffusion hanging-drop method at 20 °C. The protein concentrations of YcgR-c-di-GMP, YcgR-N, and PilZ-c-di-GMP used in crystallization were 17, 8, and 8 mg ml^{-1}, respectively. The best crystals of YcgR-c-di-GMP were obtained after 3 days in 0.2 M potassium thiocyanate, 0.1 M BisTris, pH 6.0, and 20% (w/v) PEG 3350. The crystals of YcgR SeMet derivative grew with c-di-GMP after 7 days in a condition consisting of 0.2 M sodium malonate, 0.1 M BisTris, pH 6.0, and 20% (w/v) PEG 3350, using a concentration of 20 mg ml^{-1}. The YcgR-N was crystallized after 4–5 days in 0.1 M MES, pH 5.6, 0.01 M magnesium chloride hexahydrate, and 1.8 M lithium sulfate. The crystals of PilZ-c-di-GMP used for diffraction appeared in 0.2 M

ammonium sulfate, 0.1 M BisTris, pH 5.5, and 23% PEG 3350 after about 7 days.

Prior to flash freezing in liquid nitrogen, the crystals were soaked for 30–60 s in the mother liquor solution containing 10–25% (v/v) glycerol. Diffraction data of YcgR-c-di-GMP were collected to a resolution of 2.3 Å using an ADSC Q315r CCD detector at beamline BL-17A, KEK (Photon Factory, Tsukuba, Japan) with a wavelength of 0.9791 Å. The data were integrated and scaled by MOSFLM (40) and SCALA from the CCP4 software suite (41). The space group was determined to be *R*3:*H* with one molecule per asymmetric unit. The data of SeMet-derivative crystals were collected for experimental phasing at beamline BL17U1 (42), Shanghai Synchrotron Radiation Facility (SSRF), using an ADSC Q315r CCD detector with a wavelength of 0.9793 Å. The data were processed by MOSFLM and SCALA. The phasing and the initial model building were performed by Phenix Autosol (43) using the single-wavelength anomalous diffraction method. The model was then used in Phaser from the CCP4 software suite for molecular replacement against the native data. The model was improved by iterative cycles of refinement and manual building using CNS (44), Phenix.refine (45), and Coot (46). The final model contained 226 amino acids, except the residues 123–124, 156–160, and 195–203 between two β-strands and 244 at the C terminus because of poor electron density, and two c-di-GMPs intercalated to each other.

Diffraction data of PilZ-c-di-GMP were collected at beamline BL17U1 (42) at SSRF with a wavelength of 0.9793 Å and also processed with MOSFLM (40) and SCALA (41). The crystals belonged to space group $P3_121$ and contained one copy in the asymmetric unit. The structure was solved at 2.3 Å by molecular replacement with Phaser_MR in the Phenix suite using the coordinates of C-terminal domain structure of YcgR-c-di-GMP as the search model. The final structure was obtained through iterative cycles of manual building and refinement by Phenix.autobuild (43), Phenix.refine (45), and Coot (46). The model consisted of 129 amino acids, including the missing part in the YcgR-c-di-GMP model and two intercalated c-di-GMPs.

Diffraction data of YcgR-N were collected with a wavelength of 1.5418 Å using a Rigaku MM007 CCD944+HG system at the National Laboratory of Biomacromolecules, Institute of Biophysics, and Chinese Academy of Sciences. The data were processed by MOSFLM (40) and SCALA (41). The crystals diffracted to 1.77 Å resolution and also belonged to the trigonal space group *R*3:*H*. The N-terminal domain structure of YcgR-c-di-GMP was used for molecular replacement with Phaser_MR. The refinement and manual model building were taken by Phenix.refine (45) and Coot (46). The model contained 110 amino acids, including residues 4–111, leucine, and glutamic before the His tag.

The statistics of data collection and refinement are summarized in Table S1. The structural figures were prepared with PyMOL.

Binding studies by size-exclusion chromatography

Analytical SEC experiments were performed at 16 °C on a Superdex 200 10/300 GL column (GE Healthcare) to determine the interactions between YcgR and flagellar motor proteins. Purified YcgR was mixed with MotAc, FliG, or FliMN at a 1:1 molar ratio, incubated for 30 min on ice, and then loaded on the column in a final volume of 500 μl. For the YcgR-c-di-GMP complex, 3-fold excess of c-di-GMP were first added to YcgR solution on the ice for 30 min, and then the complex was incubated with flagellar motor proteins for another 30 min. The samples were eluted in SEC buffer at a flow rate of 0.5 ml min^{-1} with monitoring of the absorbance at 280 and 254 nm. The eluted peaks were analyzed on SDS-polyacrylamide gels and stained with Coomassie Blue. The apparent masses were determined using Gel Filtration Calibration Kits (GE Healthcare) with the standard procedure on the Superdex 200 10/300 GL column. PilZ, YcgR-N, and the mutant derivatives of YcgR were assayed in the same way.

Isothermal titration calorimetry assays

ITC experiments were performed using a MicroCal iTC-200 calorimeter (Malvern) at 25 °C. c-di-GMP was dissolved and diluted in the SEC buffer. Each titration consisted of 21 or 31 injections, the first one 0.5 μl (not used in data fitting) and all subsequent injections of a 2- or 1.2-μl volume. 100–200 μM c-di-GMP solution was titrated into 5–10 μM YcgR (WT), PilZ, Q112A, QND/AAA, F117A, I228A, F229A, or E232A solutions because of the relatively high c-di-GMP affinity of those proteins. For those proteins with relatively low c-di-GMP affinity, such as R113A, R114A, R118A, D145A, S147A, R208A, or YcgR-N, 1–2 mM c-di-GMP solution was injected into the sample cell containing 30–70 μM protein solution. The titration data were integrated and fitted to a one-site model using the Origin program provided by the manufacturer. The binding constant (K_a, $K_d = 1/K_a$) and the stoichiometry (n) were extracted directly from the fit.

Small-angle X-ray scattering measurement and modeling

Synchrotron SAXS data of YcgR, YcgR-c-di-GMP, MotAc, and the complex of MotAc and YcgR-c-di-GMP were collected on beamline BL19U2 at the National Center for Protein Science Shanghai (NCPSS) at 4 °C. Scattering curves were recorded at a wavelength of 1.03 Å on a Pilatus 1M detector over an angular range of $0.013 < q < 0.4546$ Å^{-1}, where $q = (4\pi\sin\theta)/\lambda$, and 2θ is the scattering angle. The buffer used in SAXS experiment was the SEC buffer. Twenty consecutive frames of 1-s exposure time were recorded and averaged. The raw data were processed using PRIMUS (47) for background subtraction, concentration scaling, and curve merging. The data were checked for radiation damage and concentration-induced aggregation. The curve of 2 mg ml^{-1} YcgR and the curve of low-q data from 0.6 mg ml^{-1} YcgR-c-di-GMP merged with higher-q data from 4.8 mg ml^{-1} YcgR-c-di-GMP, the curve of low-q data from 5 mg ml^{-1} MotAc merged with higher-q data from 10 mg ml^{-1} MotAc, and the curve of 4 mg ml^{-1} MotAc-YcgR-c-di-GMP were used in subsequent analysis. Guinier analysis and Primus distance distribution analysis of Primus qt from the ATSAS program suite (48) were performed to calculate the radius of gyration (R_g), scattering intensity extrapolated to zero angle $I(0)$, maximum dimension D_{max}, and pair distance distribution function $P(r)$. Twenty independent *ab initio* models were com-

puted with the simulated annealing *ab initio* bead-modeling programs DAMMIF (29). The 20 models were compared using DAMSEL from the ATSAS program suite, and the most probable one was chosen to be the final SAXS envelope. The simulated scattering curves fitted to the experimental data with a discrepancy factor χ^2 of 0.841 for YcgR-c-di-GMP, χ^2 of 1.032 for YcgR, χ^2 of 0.910 for MotAc, and χ^2 of 1.057 for MotAc-YcgR-c-di-GMP (Fig. S3). The fit of the theoretical scattering curve between the crystal structure of YcgR-c-di-GMP and the experimental data was obtained using CRYSOL (49) with χ^2 of 1.231. The SAXS envelope of YcgR-c-di-GMP was superposed to the crystal structure of YcgR-c-di-GMP by SUPCOMB (50), and the superimposed model was provided using PyMOL.

The YcgR model was constructed according to the SAXS experimental data. The molecular model ensemble that best fitted the SAXS data was performed with SASREF (51), which generated molecular models from domains or subunits with known structure by rigid-body movements and rotations. The crystal structure of YcgR-N and the PilZ model without c-di-GMP, which was simulated from the C-terminal domain of the crystal structure of MrkH (Protein Data Bank code 5KED) (31) using the automated protein structure homology-modeling server SWISS-MODEL (52, 53), were used in SASREF. Contacts were defined to guarantee the connection between the C terminus of YcgR-N and the N terminus of PilZ. The SASREF modeling was repeated more than 10 times to obtain the best model that fitted the SAXS scattering data with χ^2 of 1.595. The YcgR SASREF model and the SAXS envelope of YcgR were superimposed by SUPCOMB (50) and visualized using PyMOL.

Motility assays

DNAs encoding YcgR-N, PilZ, YcgR, and its derivatives were cloned into pBBR1MCS-3 and transformed into Δ*yhjHycgR* (12). Swimming motility was assayed on soft agar plates containing 0.3% agar, 1% tryptone, and 0.5% NaCl. 1.5 μl of cell culture grown overnight at 37 °C in LB medium was spotted onto the freshly prepared plates and incubated for 6 h at 37 °C. The cultures were normalized to the same cell density of 2.0 at 600 nm. The diameters of the swimming zone around the inoculation sites were measured. At least five independent experiments were performed, and the arithmetic means ± S.D. were plotted by GraphPad Prism 6.

The expression levels of YcgR variants fused with a C-terminal HA tag *in vivo* were assayed using anti-HA antibody. The bacteria containing the plasmids of YcgR mutants were normalized to the same cell density of 2.0 at 600 nm, harvested using centrifugation, and lysed by BugBuster (Novagen) protein extraction reagent. The supernatants were examined by SDS-PAGE (15% acrylamide), transferred to nitrocellulose membrane, and immunoblotted with an anti-HA antibody (Cell Signaling Technology). The exposure intensity of the bands was calculated using ImageJ.

Accession numbers

Atomic coordinates and structure factors of YcgR-c-di-GMP, PilZ-c-di-GMP, and YcgR-N have been deposited in the Protein Data Bank with accession codes 5Y6F, 5Y6G, and 5Y6H, respectively. The SAXS data and structural models have been deposited at SASBDB with accession numbers SASDEB9 (YcgR) and SASDEC9 (YcgR-c-di-GMP).

Author contributions—Y.-J. H., W.-S. Y., Y. H., and D.-F. L. data curation; Y.-J. H. and D.-F. L. formal analysis; Y.-J. H., D.-C. W., and D.-F. L. funding acquisition; Y.-J. H., W.-S. Y., Y. H., and Y. Z. investigation; Y.-J. H. visualization; Y.-J. H. and D.-F. L. writing-original draft; Y.-J. H. and D.-F. L. writing-review and editing; D.-C. W. and D.-F. L. supervision; D.-C. W. and D.-F. L. validation; D.-C. W. and D.-F. L. project administration; D.-F. L. conceptualization.

Acknowledgments—We thank the staff members of beamline BL-17A at Photon Factory, KEK, beamline BL17U1 at the Shanghai Synchrotron Radiation Facility (SSRF), and beamline BL19U2 at the National Center for Protein Sciences Shanghai (NCPSS) for technical assistance in data collection. We thank Yi Han of the Protein Platform of the Institute of Biophysics for providing the in-house X-ray facility for data collection. We are grateful to Xin Fang and Mark Gomelsky for providing the strains of ΔyhjH and ΔyhjHΔycgR and to Zhou Huang for the plasmid used in the motility assays.

References

1. Hengge, R. (2009) Principles of c-di-GMP signalling in bacteria. *Nat. Rev. Microbiol.* **7,** 263–273 CrossRef Medline
2. Römling, U., Galperin, M. Y., and Gomelsky, M. (2013) Cyclic di-GMP: the first 25 years of a universal bacterial second messenger. *Microbiol. Mol. Biol. Rev.* **77,** 1–52 CrossRef Medline
3. Pultz, I. S., Christen, M., Kulasekara, H. D., Kennard, A., Kulasekara, B., and Miller, S. I. (2012) The response threshold of *Salmonella* PilZ domain proteins is determined by their binding affinities for c-di-GMP. *Mol. Microbiol.* **86,** 1424–1440 CrossRef Medline
4. Jenal, U., Reinders, A., and Lori, C. (2017) Cyclic di-GMP: second messenger extraordinaire. *Nat. Rev. Microbiol.* **15,** 271–284 CrossRef Medline
5. Schirmer, T., and Jenal, U. (2009) Structural and mechanistic determinants of c-di-GMP signalling. *Nat. Rev. Microbiol.* **7,** 724–735 CrossRef Medline
6. Jenal, U., and Malone, J. (2006) Mechanisms of cyclic-di-GMP signaling in bacteria. *Annu. Rev. Genet.* **40,** 385–407 CrossRef Medline
7. Boehm, A., Kaiser, M., Li, H., Spangler, C., Kasper, C. A., Ackermann, M., Kaever, V., Sourjik, V., Roth, V., and Jenal, U. (2010) Second messenger-mediated adjustment of bacterial swimming velocity. *Cell* **141,** 107–116 CrossRef Medline
8. Ryjenkov, D. A., Simm, R., Römling, U., and Gomelsky, M. (2006) The PilZ domain is a receptor for the second messenger c-di-GMP: the PilZ domain protein YcgR controls motility in enterobacteria. *J. Biol. Chem.* **281,** 30310–30314 CrossRef Medline
9. Ko, M., and Park, C. (2000) Two novel flagellar components and H-NS are involved in the motor function of *Escherichia coli*. *J. Mol. Biol.* **303,** 371–382 CrossRef Medline
10. Amikam, D., and Galperin, M. Y. (2006) PilZ domain is part of the bacterial c-di-GMP binding protein. *Bioinformatics* **22,** 3–6 CrossRef Medline
11. Paul, K., Nieto, V., Carlquist, W. C., Blair, D. F., and Harshey, R. M. (2010) The c-di-GMP binding protein YcgR controls flagellar motor direction and speed to affect chemotaxis by a "backstop brake" mechanism. *Mol. Cell* **38,** 128–139 CrossRef Medline
12. Fang, X., and Gomelsky, M. (2010) A post-translational, c-di-GMP-dependent mechanism regulating flagellar motility. *Mol. Microbiol.* **76,** 1295–1305 CrossRef Medline
13. Wolfe, A. J., and Visick, K. L. (2008) Get the message out: cyclic-di-GMP regulates multiple levels of flagellum-based motility. *J. Bacteriol.* **190,** 463–475 CrossRef Medline
14. Berg, H. C. (2003) The rotary motor of bacterial flagella. *Annu. Rev. Biochem.* **72,** 19–54 CrossRef Medline
15. Reid, S. W., Leake, M. C., Chandler, J. H., Lo, C. J., Armitage, J. P., and Berry, R. M. (2006) The maximum number of torque-generating units in

the flagellar motor of *Escherichia coli* is at least 11. *Proc. Natl. Acad. Sci. U.S.A.* **103,** 8066–8071 CrossRef Medline

16. Braun, T. F., Al-Mawsawi, L. Q., Kojima, S., and Blair, D. F. (2004) Arrangement of core membrane segments in the MotA/MotB proton-channel complex of *Escherichia coli*. *Biochemistry* **43,** 35–45 CrossRef Medline
17. Paul, K., Gonzalez-Bonet, G., Bilwes, A. M., Crane, B. R., and Blair, D. (2011) Architecture of the flagellar rotor. *EMBO J.* **30,** 2962–2971 CrossRef Medline
18. Zhou, J., Lloyd, S. A., and Blair, D. F. (1998) Electrostatic interactions between rotor and stator in the bacterial flagellar motor. *Proc. Natl. Acad. Sci. U.S.A.* **95,** 6436–6441 CrossRef Medline
19. Bren, A., and Eisenbach, M. (1998) The N terminus of the flagellar switch protein, FliM, is the binding domain for the chemotactic response regulator, CheY. *J. Mol. Biol.* **278,** 507–514 CrossRef Medline
20. Sarkar, M. K., Paul, K., and Blair, D. (2010) Chemotaxis signaling protein CheY binds to the rotor protein FliN to control the direction of flagellar rotation in *Escherichia coli*. *Proc. Natl. Acad. Sci. U.S.A.* **107,** 9370–9375 CrossRef Medline
21. Blair, K. M., Turner, L., Winkelman, J. T., Berg, H. C., and Kearns, D. B. (2008) A molecular clutch disables flagella in the *Bacillus subtilis* biofilm. *Science* **320,** 1636–1638 CrossRef Medline
22. Guttenplan, S. B., Blair, K. M., and Kearns, D. B. (2010) The EpsE flagellar clutch is bifunctional and synergizes with EPS biosynthesis to promote *Bacillus subtilis* biofilm formation. *PLoS Genet.* **6,** e1001243 CrossRef Medline
23. Armitage, J. P., and Berry, R. M. (2010) Time for bacteria to slow down. *Cell* **141,** 24–26 CrossRef Medline
24. Brown, M. T., Delalez, N. J., and Armitage, J. P. (2011) Protein dynamics and mechanisms controlling the rotational behaviour of the bacterial flagellar motor. *Curr. Opin. Microbiol.* **14,** 734–740 CrossRef Medline
25. Hou, Y., Li, D.-F., and Wang, D.-C. (2013) Crystallization and preliminary X-ray analysis of the flagellar motor "brake" molecule YcgR with c-di-GMP from *Escherichia coli*. *Acta Crystallogr. Sect. F Struct. Biol. Cryst. Commun.* **69,** 663–665 CrossRef Medline
26. Dean, G. E., Macnab, R. M., Stader, J., Matsumura, P., and Burks, C. (1984) Gene sequence and predicted amino acid sequence of the motA protein, a membrane-associated protein required for flagellar rotation in *Escherichia coli*. *J. Bacteriol.* **159,** 991–999 Medline
27. Zhou, J., Fazzio, R. T., and Blair, D. F. (1995) Membrane topology of the MotA protein of *Escherichia coli*. *J. Mol. Biol.* **251,** 237–242 CrossRef Medline
28. Takekawa, N., Terahara, N., Kato, T., Gohara, M., Mayanagi, K., Hijikata, A., Onoue, Y., Kojima, S., Shirai, T., Namba, K., and Homma, M. (2016) The tetrameric MotA complex as the core of the flagellar motor stator from hyperthermophilic bacterium. *Sci. Rep.* **6,** 31526 CrossRef Medline
29. Franke, D., and Svergun, D. I. (2009) DAMMIF, a program for rapid *ab-initio* shape determination in small-angle scattering. *J. Appl. Crystallogr.* **42,** 342–346 CrossRef Medline
30. Ko, J., Ryu, K. S., Kim, H., Shin, J. S., Lee, J. O., Cheong, C., and Choi, B. S. (2010) Structure of PP4397 reveals the molecular basis for different c-di-GMP binding modes by PilZ domain proteins. *J. Mol. Biol.* **398,** 97–110 CrossRef Medline
31. Schumacher, M. A., and Zeng, W. (2016) Structures of the activator of *K. pneumonia* biofilm formation, MrkH, indicates PilZ domains involved in c-di-GMP and DNA binding. *Proc. Natl. Acad. Sci. U.S.A.* **113,** 10067–10072 CrossRef Medline
32. Wang, F., He, Q., Su, K., Gao, F., Huang, Y., Lin, Z., Zhu, D., and Gu, L. (2016) The PilZ domain of MrkH represents a novel DNA binding motif. *Protein Cell* **7,** 766–772 CrossRef Medline
33. Subramanian, S., Gao, X., Dann, C. E., 3rd, and Kearns, D. B. (2017) MotI (DgrA) acts as a molecular clutch on the flagellar stator protein MotA in *Bacillus subtilis*. *Proc. Natl. Acad. Sci.* **114,** 13537–13542 CrossRef Medline
34. Benach, J., Swaminathan, S. S., Tamayo, R., Handelman, S. K., Folta-Stogniew, E., Ramos, J. E., Forouhar, F., Neely, H., Seetharaman, J., Camilli, A., and Hunt, J. F. (2007) The structural basis of cyclic diguanylate signal transduction by PilZ domains. *EMBO J.* **26,** 5153–5166 CrossRef Medline
35. Baker, A. E., Diepold, A., Kuchma, S. L., Scott, J. E., Ha, D. G., Orazi, G., Armitage, J. P., and O'Toole, G. A. (2016) PilZ domain protein FlgZ mediates cyclic di-GMP-dependent swarming motility control in *Pseudomonas aeruginosa*. *J. Bacteriol.* **198,** 1837–1846 CrossRef Medline
36. Mathews, M. A. A., Tang, H. L., and Blair, D. F. (1998) Domain analysis of the FliM protein of *Escherichia coli*. *J. Bacteriol.* **180,** 5580–5590 Medline
37. Kovach, M. E., Elzer, P. H., Steven Hill, D. S., Robertson, G. T., Farris, M. A., Roop, R. M., 2nd, and Peterson, K. M. (1995) Four new derivatives of the broad-host-range cloning vector pBBR1MCS, carrying different antibiotic-resistance cassettes. *Gene* **166,** 175–176 CrossRef Medline
38. Sawano, A., and Miyawaki, A. (2000) Directed evolution of green fluorescent protein by a new versatile PCR strategy for site-directed and semi-random mutagenesis. *Nucleic Acids Res.* **28,** E78 CrossRef Medline
39. Schuck, P. (2000) Size-distribution analysis of macromolecules by sedimentation velocity ultracentrifugation and Lamm equation modeling. *Biophys. J.* **78,** 1606–1619 CrossRef Medline
40. Battye, T. G. G., Kontogiannis, L., Johnson, O., Powell, H. R., and Leslie, A. G. W. (2011) iMOSFLM: a new graphical interface for diffraction-image processing with MOSFLM. *Acta Crystallogr. D Biol. Crystallogr.* **67,** 271–281 CrossRef Medline
41. Winn, M. D., Ballard, C. C., Cowtan, K. D., Dodson, E. J., Emsley, P., Evans, P. R., Keegan, R. M., Krissinel, E. B., Leslie, A. G. W., McCoy, A., McNicholas, S. J., Murshudov, G. N., Pannu, N. S., Potterton, E. A., Powell, H. R., *et al.* (2011) Overview of the CCP4 suite and current developments. *Acta Crystallogr. D Biol. Crystallogr.* **67,** 235–242 CrossRef Medline
42. Qi-Sheng, W., Feng, Y., Sheng, H., Bo, S., Kun-Hao, Z., Ke, L., Zhi-Jun, W., Chun-yan, X., Si-Sheng, W., Li-Feng, Y., Qiang-Yan, P., Liang, L., Huan, Z., Yin, C., Qin, X., Earnest, T., and Jian-Hua, H. (2015) The macromolecular crystallography beamline of SSRF. *Nuclear Sci. Techniques* **26,** 12–17 CrossRef
43. Terwilliger, T. C., Adams, P. D., Read, R. J., McCoy, A. J., Moriarty, N. W., Grosse-Kunstleve, R. W., Afonine, P. V., Zwart, P. H., and Hung, L.-W. (2009) Decision-making in structure solution using Bayesian estimates of map quality: the PHENIX AutoSol wizard. *Acta Crystallogr. D Biol. Crystallogr.* **65,** 582–601 CrossRef Medline
44. Brünger, A. T., Adams, P. D., Clore, G. M., DeLano, W. L., Gros, P., Grosse-Kunstleve, R. W., Jiang, J.-S., Kuszewski, J., Nilges, M., Pannu, N. S., Read, R. J., Rice, L. M., Simonson, T., and Warren, G. L. (1998) Crystallography and NMR system: a new software suite for macromolecular structure determination. *Acta Crystallogr. D Biol. Crystallogr.* **54,** 905–921 CrossRef Medline
45. Adams, P. D., Afonine, P. V., Bunkóczi, G., Chen, V. B., Davis, I. W., Echols, N., Headd, J. J., Hung, L.-W., Kapral, G. J., Grosse-Kunstleve, R. W., McCoy, A. J., Moriarty, N. W., Oeffner, R., Read, R. J., Richardson, D. C., *et al.* (2010) PHENIX: a comprehensive Python-based system for macromolecular structure solution. *Acta Crystallogr. D Biol. Crystallogr.* **66,** 213–221 CrossRef Medline
46. Emsley, P., Lohkamp, B., Scott, W. G., and Cowtan, K. (2010) Features and development of Coot. *Acta Crystallogr. D Biol. Crystallogr.* **66,** 486–501 CrossRef Medline
47. Konarev, P. V., Volkov, V. V., Sokolova, A. V., Koch, M. H. J., and Svergun, D. I. (2003) PRIMUS: a Windows PC-based system for small-angle scattering data analysis. *J. Appl. Crystallogr.* **36,** 1277–1282 CrossRef
48. Petoukhov, M. V., Franke, D., Shkumatov, A. V., Tria, G., Kikhney, A. G., Gajda, M., Gorba, C., Mertens, H. D. T., Konarev, P. V., and Svergun, D. I. (2012) New developments in the ATSAS program package for small-angle scattering data analysis. *J. Appl. Crystallogr.* **45,** 342–350 CrossRef Medline
49. Svergun, D., Barberato, C., and Koch, M. H. J. (1995) CRYSOL—a program to evaluate X-ray solution scattering of biological macromolecules from atomic coordinates. *J. Appl. Crystallogr.* **28,** 768–773 CrossRef
50. Kozin, M. B., and Svergun, D. I. (2001) Automated matching of high- and low-resolution structural models. *J. Appl. Crystallogr.* **34,** 33–41 CrossRef

51. Petoukhov, M. V., and Svergun, D. I. (2005) Global rigid body modeling of macromolecular complexes against small-angle scattering data. *Biophys. J.* **89,** 1237–1250 CrossRef Medline
52. Arnold, K., Bordoli, L., Kopp, J., and Schwede, T. (2006) The SWISS-MODEL workspace: a web-based environment for protein structure homology modelling. *Bioinformatics* **22,** 195–201 CrossRef Medline
53. Biasini, M., Bienert, S., Waterhouse, A., Arnold, K., Studer, G., Schmidt, T., Kiefer, F., Gallo Cassarino, T., Bertoni, M., Bordoli, L., and Schwede, T. (2014) SWISS-MODEL: modelling protein tertiary and quaternary structure using evolutionary information. *Nucleic Acids Res.* **42,** W252–W258 CrossRef Medline
54. Ashkenazy, H., Abadi, S., Martz, E., Chay, O., Mayrose, I., Pupko, T., and Ben-Tal, N. (2016) ConSurf 2016: an improved methodology to estimate and visualize evolutionary conservation in macromolecules. *Nucleic Acids Res.* **44,** W344–W350 CrossRef Medline
55. Crooks, G. E., Hon, G., Chandonia, J.-M., and Brenner, S. E. (2004) WebLogo: a sequence logo generator. *Genome Res.* **14,** 1188–1190 CrossRef Medline